Electronic Supplementary Material (ESI) for Analyst.

Supporting Information

Electrochemical Detection of Alzheimer's Disease Related Substances in Biofluids by Silica Nanochannel Membrane Modified Glassy Carbon Electrodes

Lin Zhou, Hao Ding, Fei Yan, Weiliang Guo and Bin Su*

Institute of Analytical Chemistry, Department of Chemistry, Zhejiang University, Hangzhou, 310058, China

Table of Contents

S1. SNM/GCE Preparation

The preparation of SNM/GCE involved the following steps:

(a) APTES was electrografted on the GCE surface as the molecular glue between GCE and SNM to improve the mechanical stability of prepared SNM.

(b) SNM/GCE with surfactants (designated as SMs@SNM/GCE) was prepared using the Electro-Assisted Self-Assembly (EASA) method.

(c) SNM/GCE with open channels was obtained by immersing the electrode in 0.1 M HCl ethanol solution for 15 min.

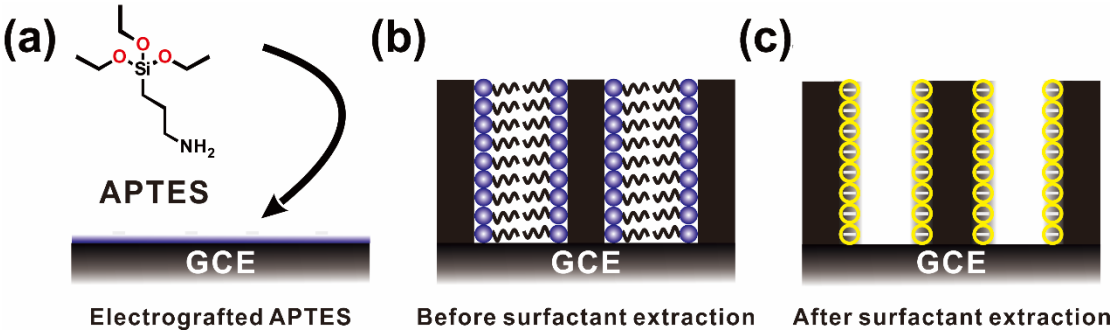

Scheme S1 Illustration of preparation of SNM/GCE

S2. SEM Characterization

Fig. S1a shows the top-view SEM image of the newly polished GCE surface. It is clear that the surface is pretty smooth. After electrografting with APTES, some white particles were generated on the GCE surface, which was mostly generated by hydrolyzation of APTES under air conditions (**Fig. S1b**). After further growing SNM on the surface, some bigger particles were generated on the top surface of SNM (**Fig. S1c**). As reported previously,[S1] these particles are most likely silica nanoparticle byproducts.

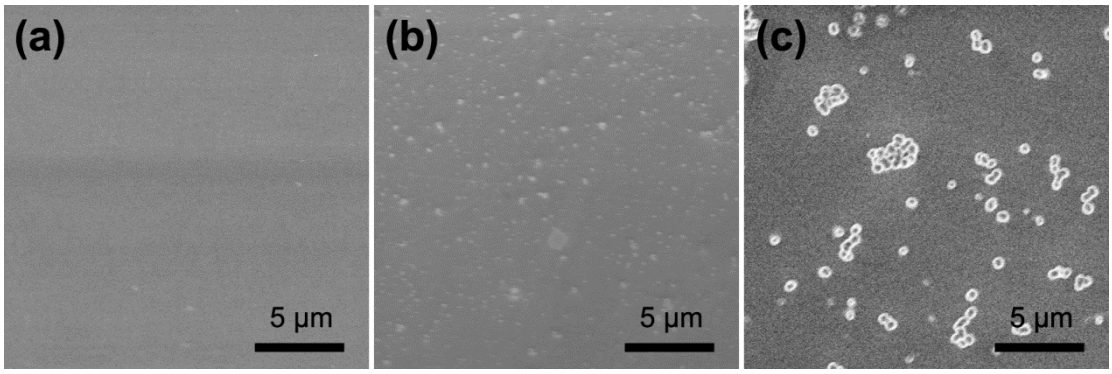

Fig. S1. Top-view SEM images of GCE (a), GCE electrografted with APTES (APTES/GCE) (b) and SNM/GCE (c).

S3. Electrochemistry Characterization

Fig. S2 shows CVs of $Ru(NH_3)_6^{3+}$ obtained with a bare GCE, SNM/GCE with surfactants (SMs@SNM/GCE) and SNM/GCE.

Given the surfactants formed micelles inside nanochannels, the hydrophobic cores of micelles could blocked the access and mass transport of hydrophilic, charged $Ru(NH_3)_6^{3+}$ from bulk solution to underlying GCE surface, yielding a featureless capacitive current (black curve). This response also indicated that the as-prepared SNM was compact without leakage or cracks.

After excluding the surfactants from SNM, the redox reaction of $Ru(NH_3)_6^{3+}$ at the SNM/GCE yielded a CV similar to the bare GCE (blue and red curves), indicating the SNM was highly permeable. Considering the effective electrode surface area was decreased by roughly 80%, a comparable current magnitude suggested the enhanced mass transport of $Ru(NH_3)_6^{3+}$ at the SNM/GCE.

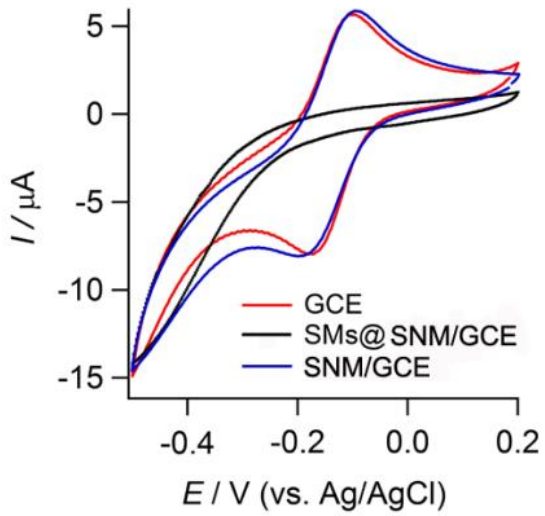

Fig. S2 CVs obtained at the GCE, SNM/GCE with surfactants (designated as SMs@SNM/GCE) and SNM/GCE in 0.1 M KCl containing 0.5 mM $Ru(NH_3)_6Cl_3$. The scan rate was 100 mV/s.

S4. Stripping Analysis of Cu^{2+}

We believe the negatively charged surface of SNM can electrostatically enrich Cu^{2+}. The solution pH and electrodeposition time were firstly optimized to obtain a sensitive analysis.

As shown in **Fig. S3a**, the stripping current reached the maximum at a pH ranging from 6.0 to 8.0. Note that at an even higher pH silica is not stable and at a lower pH the electrostatic interaction is weak.

As seen from **Fig. S3b**, the stripping current sharply increased with increasing the electrodeposition time from 0 to 300 s and eventually reached a plateau beyond 300 s.

Therefore, the optimal pH and electrodeposition time was set to 6.0 and 300 s, respectively, for the stripping analysis of Cu^{2+}.

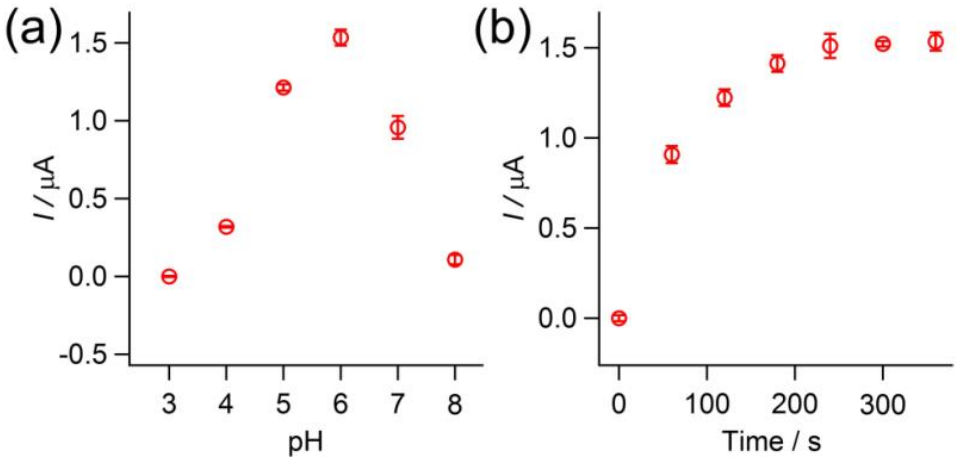

Fig. S3 The effect of solution pH (a) and electrodeposition time (b) on the stripping current signals for the detection of 1.0 μM Cu^{2+} using the SNM/GCE.

S5. Voltammetry Analysis of DA

Fig. S4a shows the CVs of DA at the SNM/GCE in 0.1 M PBS at different pH. Apparently, the current wave shifted negatively with increasing the solution pH. **Fig. S4b** shows the dependence of anodic peak potential on the solution pH, yielding a slope of −0.061 V/pH and suggesting a proton-coupled electron transfer process by a proton/electron ratio of 1.

Fig. S4c shows the variation of oxidation peak current at different pH. A maximum current magnitude was observed at pH 6.0. **Fig. S5** shows that the peak currents linearly increase with the square root of scan rate in the range from 10 to 500 mV s^{-1}, suggesting a diffusion controlled process.

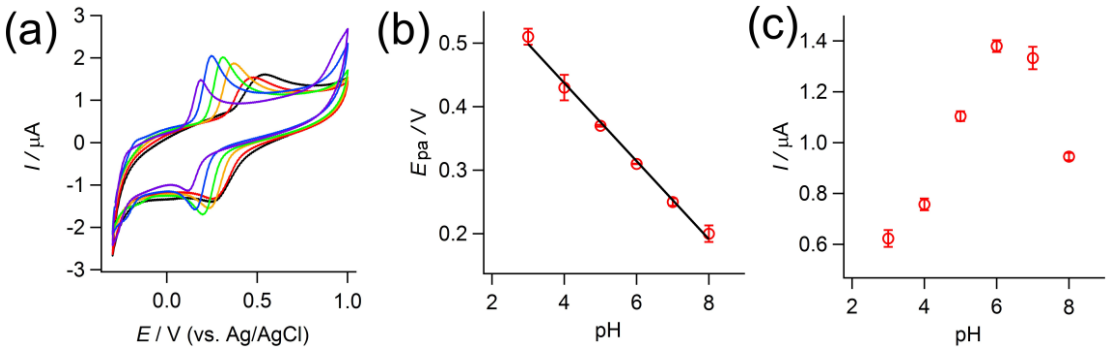

Fig. S4 (a) CVs obtained at a SNM/GCE in 0.1 M PBS containing 50 μM DA at different pH values. (b) The calibration curve of the oxidation peak potential with pH. The straight line corresponds to a linear fitting with a slope of 0.061 V/pH. (c) The oxidation peak current obtained at the SNM/GCE with 50 μM DA in 0.1 M PBS at different pH.

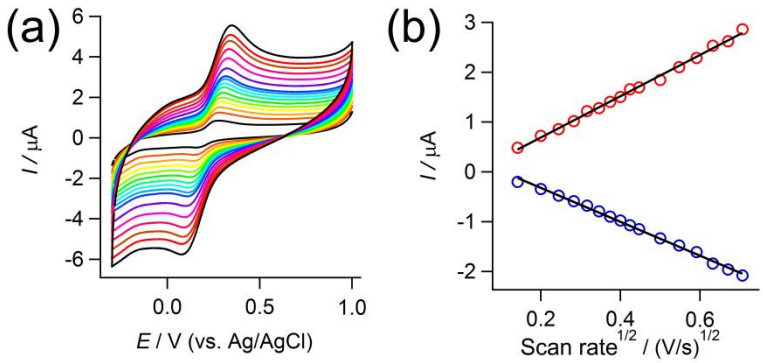

Fig. S5 (a) CVs obtained at the SNM/GCE at different scan rates (10 mV/s to 500 mV/s) in 0.1 M PBS containing 50 μM DA. (b) The dependence of peak current currents on the square root of scan rate.

S6. DA Analysis by ECL-Intensity Mode

S6.1 Optimal $Ru(bpy)_3^{2+}$ and TPrA Concentrations

ECL analysis of DA was performed in two different modes.

The intensity mode was carried out by measuring the variation of ECL intensity of $Ru(bpy)_3^{2+}$/TPrA system in the presence of DA. DA has been reported to be a quencher of this ECL reaction system.

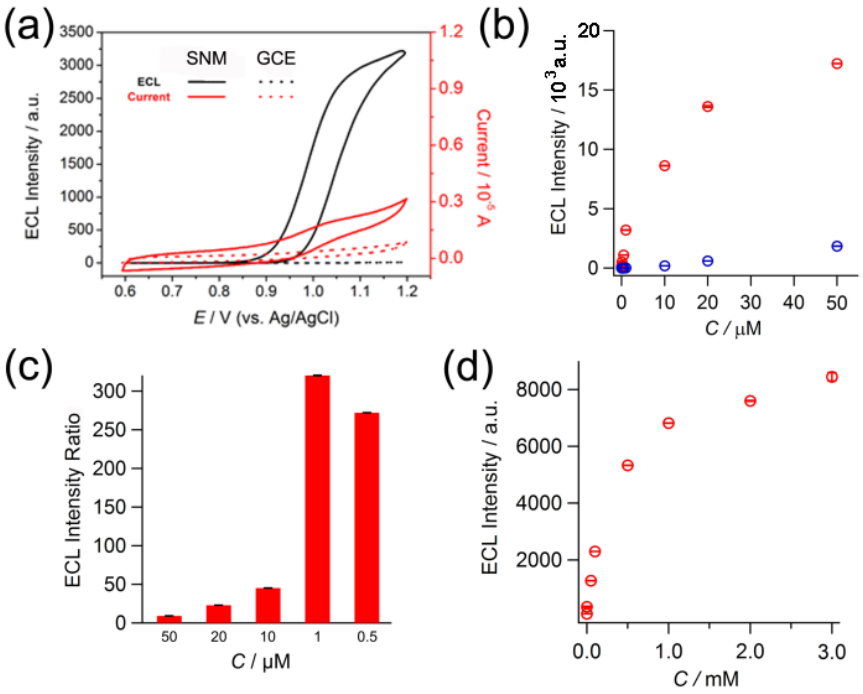

Fig. S6 (a) CVs (red) and ECL-voltage curves (black) recorded in 0.1 M PBS (pH 6.0) containing 1 μM $Ru(bpy)_3^{2+}$ and 3 mM TPrA at the SNM/GCE (solid line) and GCE (dotted line). The potential scan rate was 100 mV/s. (b) Dependence of ECL intensity on the concentration of $Ru(bpy)_3^{2+}$ at the SNM/GCE (red) and GCE (blue). The solution was 0.1 M PBS (pH 6.0) containing 3 mM TPrA. (c) The magnification of ECL intensity at various concentrations of $Ru(bpy)_3^{2+}$ (ECL intensity ratio was $ECL_{SNM/GCE}/ECL_{GCE}$). The solution was 0.1 M PBS (pH 6.0) containing 3 mM TPrA. (d) Dependence of ECL intensity on the concentration of TPrA at the SNM/GCE. The solution was 0.1 M PBS (pH 6.0) containing 10 μM $Ru(bpy)_3^{2+}$. In all cases, the PMT voltage was biased at 450 V.

The ECL generation by $Ru(bpy)_3^{2+}$/TPrA at the SNM/GCE was firstly studied. As shown in **Fig. S6a**, when the potential was swept beyond +0.9 V, an obvious ECL signal could be observed. In 0.1 M PBS (pH 6.0) containing 1 μM $Ru(bpy)_3^{2+}$ and 3 mM TPrA, the

ECL intensity obtained at the SNM/GCE was 320 times larger than GCE. This enhancement can be most likely ascribed to the electrostatic effect of negatively charged surface of SNM.

Fig. S6b compares the ECL intensity generated at the SNM/GCE and GCE for different concentrations of $Ru(bpy)_3^{2+}$ when the solution contained a constant excess amount of TPrA (namely 3 mM). Apparently, the ECL intensity increased with increasing the concentration of $Ru(bpy)_3^{2+}$ in both cases. Moreover, the overall ECL intensity at the SNM/GCE was much higher than GCE. **Fig. S6c** illustrates the ratio of ECL intensities measured at two electrodes, which can be defined as the ECL enhancement factor. It can be seen that when the concentration of $Ru(bpy)_3^{2+}$ was 1 μM the enhancement factor reached the maximum, namely 320. However, at this concentration the absolute ECL intensity detected at the SNM/GCE was not high enough, therefore a concentration of 10 μM was used in the analysis of DA.

Fig. S6d displays the variation of ECL intensity with the concentration of TPrA in the presence of 10 μM $Ru(bpy)_3^{2+}$. The ECL intensity increased sharply when the concentration of TPrA was lower than 1 mM and slowly above 1 mM. Considering a high concentration of TPrA might increase the background noise, the concentration of TPrA was fixed at 1 mM in the analysis of DA.

S6.2 Optimal Solution pH for Double-Potential Step ECL Measurements

The ECL reaction of $Ru(bpy)_3^{2+}$/TPrA system is also dependent on pH. A higher pH favors the generation of TPrA radical species and thus results in a higher ECL intensity. However, **Fig. S4** shows that at a higher pH the oxidation current of DA decreases, because the oxidation-polymerization of DA occurs.

Fig. S7a compares the ECL intensities of SNM/GCE at different pH in the absence and presence of 1.0 μM DA. Apparently, the presence of DA leads to the decrease of ECL intensity. We define here the quenching ratio as,

$$r_q = \frac{I_{absence} - I_{presence}}{I_{absence}} \quad \text{(S1)}$$

where $I_{absence}$ and $I_{presence}$ denote the ECL intensity in the absence and presence of DA. As shown in **Fig. S7b**, a maximum r_q of 33% was obtained at pH 7.0. In other words, the addition of DA leads to a decrease of ECL intensity to 67% of its initial value. Therefore, the solution pH was controlled at 7.0 for the analysis of DA in the double-potential step measurement (see **Fig. 4** in the manuscript).

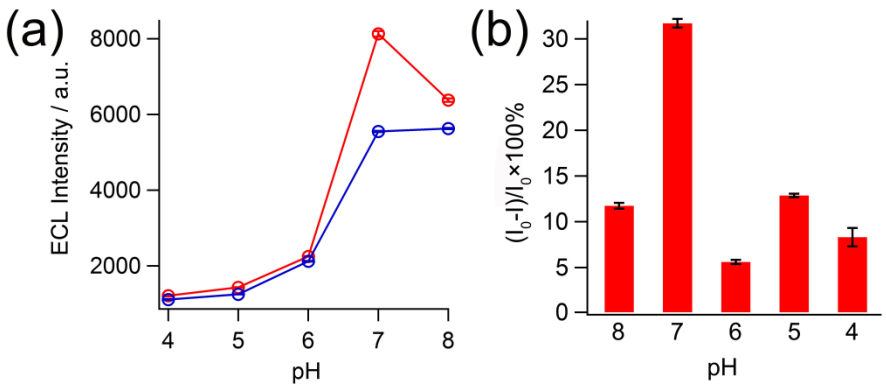

Fig. S7 (a) pH effect on the ECL intensity of SNM/GCE in the absence (red) and presence (blue) of 1.0 μM DA. The solution was 0.1 M PBS at different pH. The concentration of $Ru(bpy)_3Cl_2$ and TPrA was 10 μM and 1 mM. The PMT voltage was biased at 450 V. (b) The ECL quenching ratio of DA at the SNM/GCE.

S7. DA Analysis by ECL-Image Mode

Fig. S8 compares the ECL images of SNM/GCE and GCE captured at different potentials. At the SNM/GCE, bright image appeared at a potential more positive than +1.0 V, at which the GCE remained dark until the potential was beyond +1.2 V, indicating a higher sensitivity of the former electrode. This is similar to that observed in the intensity mode.

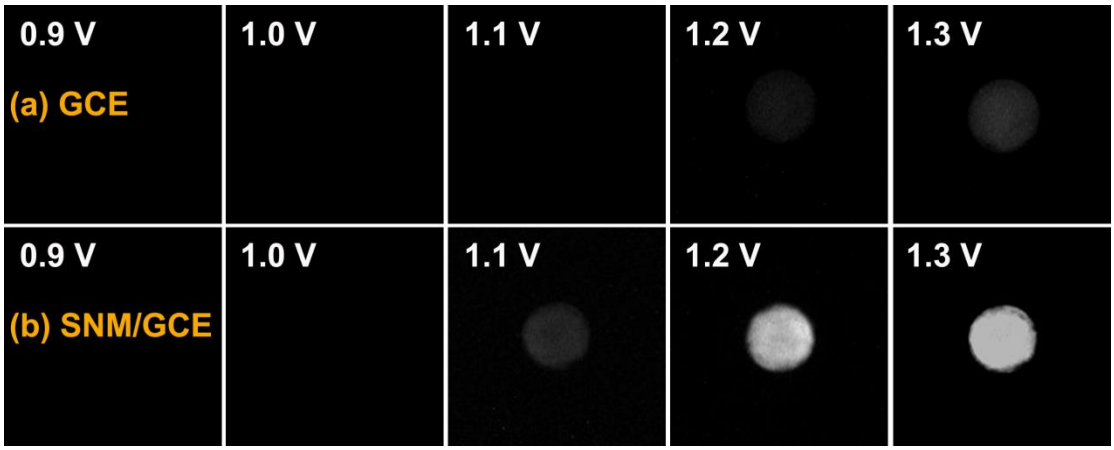

Fig. S8 ECL images obtained at GCE (a) and SNM/GCE (b) at different potentials in the course of potential scanning from +1.0 to +1.3 V. The scan rate was 0.1 V s^{-1} and the CCD exposure time was 12 s.

S8. Stability

Fig. S9 illustrates the current values of SNM/GCE in the detection of Cu^{2+} and DA using stripping voltammetry and DPV for ten times. Apparently, the current is pretty stable with a variation less than 10%, indicating the electrode is can be repeatedly used with a satisfied stability.

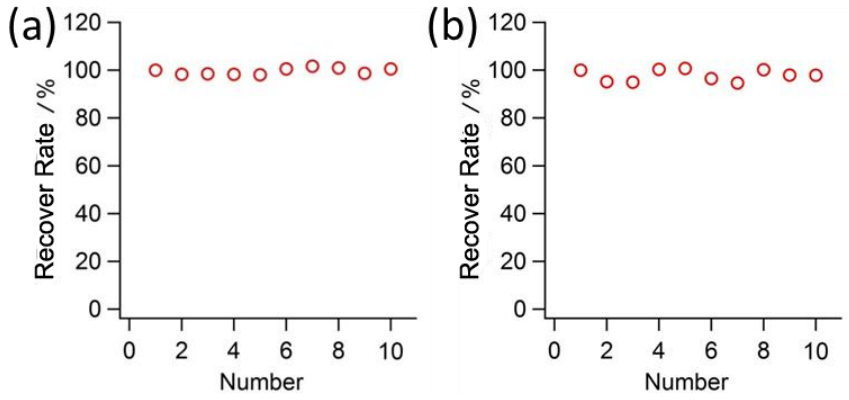

Fig. S9 The reusability of SNM/GCE in the detection of 1 μM Cu^{2+} by stripping voltammetry (a) and 50 μM DA by DPV (b). The initial current in the first detection is set as 100 %.

S9. Biofluid Analysis

S9.1 Detection of DA in ACSF

Fig. S10 and **S11** compare DPV curves and ECL intensity curves obtained at the SNM/GCE and GCE in ACSF containing different amount of DA.

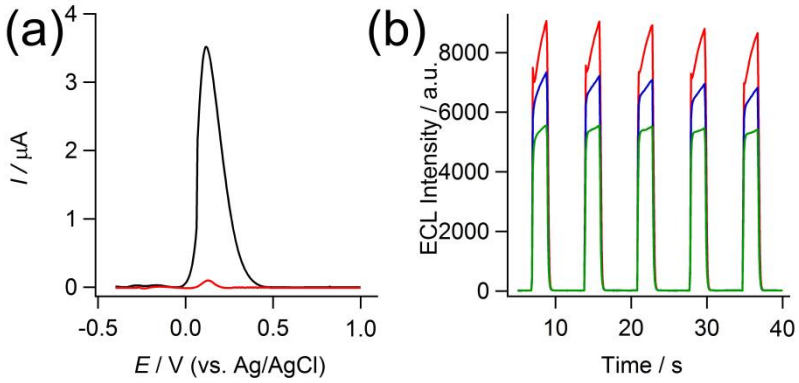

Fig. S10 (a) DPV curves of SNM/GCE in ACSF containing 200 nM DA (red line) and 50 μM DA (black line). (b) ECL intensity of SNM/GCE in ACSF in the absence (red) and presence of 30 nM DA (blue line) and 1 μM DA (green line). The concentration of $Ru(bpy)_3^{2+}$ and TPrA was 10 μM and 1 mM, respectively. The PMT voltage was biased at 450 V.

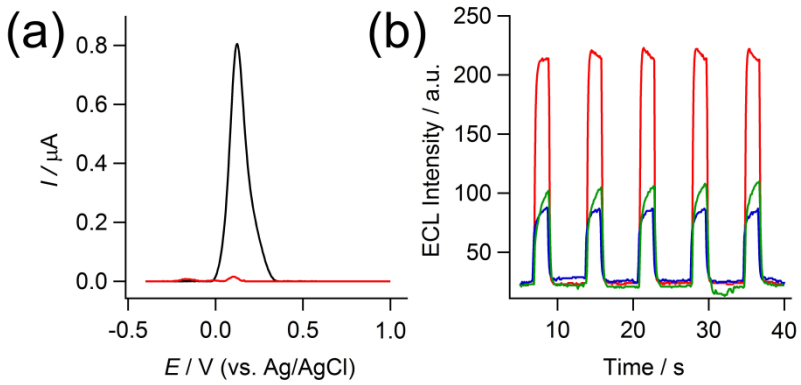

Fig. S11 (a) DPV curves of GCE in ACSF containing 200 nM DA (red line) and 50 μM DA (black line). (b) ECL intensity of GCE in ACSF in the absence (red) and presence of 30 nM DA (blue line) and 1 μM DA (green line). The concentration of $Ru(bpy)_3^{2+}$ and TPrA was 10 μM and 1 mM, respectively. The PMT voltage was biased at 450 V.

S9.3 Detection of DA in HB

Fig. S12 compares the DPV responces obtained at SNM/GCE and GCE in HB containing 40 µM DA. A sharp DA response is obtained at the SNM/GCE. Owing to severe surface befouling, only a board peak is observed at the GCE (the broad peak might also include signals of other redox species, such as UA).

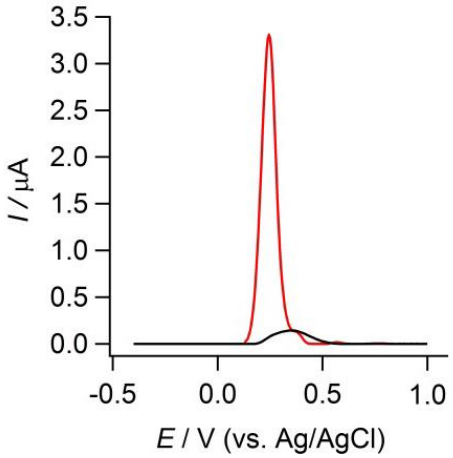

Fig. S12 DPV responses of SNM/GCE (red line) and GCE (black line) in HB (diluted 100 times by 0.01 M PBS at pH 6.0) containing 40 µM DA.

S10. Analytical data compared with previous works

Table S1 summarizes analytical data obtained with different forms of SNM modified electrodes for detecting Cu^{2+} and DA.

Table S1 Analytical data for the detection of $Cu^{2+}$and DA using different SNM modified electrodes

Electrode	Targets	Method	Potential	Sensitivity	LOD	Linear Range	Ref
SNM/GCE	Cu^{2+}	DPV	0.0 V	510 μA/μM (0.2 nM ~ 1.0 nM) 0.047 μA/μM (1.0 nM ~ 25 μM)	131 pM	200 pM ~ 25 μM	**This work**
	DA		0.23 V	0.51 μA/μM (10 nM ~ 0.8 μM) 0.064 μA/μM (0.8 μM ~ 100 μM)	7.8 nM	10 nM ~ 100 μM	
	DA	ECL	–	24200 μM^{-1} (5 nM ~ 50 nM) 1424 μM^{-1} (50 nM ~ 3 μM)	0.21 nM	5 nM ~ 3 μM	
SNM/ITO	Cu^{2+}	DPV	−0.1 V	–	20 nM	100 nM ~ 30 μM	Ref. s2
DNAzyme-based molecular gate modified SNM/ITO	Cu^{2+}	SWV	–	0.2 μA/μM	3.9 μM	4.8 μM ~ 70.2 μM	Ref. s3
Amine-functionalized SNM coated gold compact disk electrodes	Cu^{2+}	ASDPV	0.4 V	–	40 nM	0.1 ~ 10 μM	Ref. s4
SNM/ITO	DA	DPV	1.1 V	0.03 μA/μM	9 μM	20 μM ~ 226 μM	Ref. s5
Amine-functionalised SNM modified Carbon Paste Electrodes	Cu^{2+}	ASV	0.1 V	–	–	–	Ref. s6
SNM Carbon Paste Electrode	Cu^{2+}	SWV	0.1 V	–	2 nM	5 nM ~ 5 μM	Ref. s7

References

S1 *T. Nasir, L. Zhang, N. Vila, G. Herzog and A. Walcarius, Langmuir, 2016,* ***32****, 4323-4332.*

s2 *B. Cheng, L. Zhou, L. Lu, J. Liu, X. Dong, F. Xi and P. Chen, Sens. Actuators, B, 2018,* ***259****, 364-371.*

s3 *M. Saadaoui, I. Fernández, A. Sánchez, P. Díez, S. Campuzano, N. Raouafi, J. M. Pingarrón and R. Villalonga, Electrochem. Commun., 2015,* ***58****, 57-61.*

s4 *A. Walcarius and E. Sibottier, Electroanalysis, 2005,* ***17****, 1716-1726.*

s5 *W. Li, L. Ding, Q. Wang and B. Su, Analyst, 2014,* ***139****, 3926-3931.*

s6 *S. Sayen and A. Walcarius, J. Electroanal. Chem., 2005,* ***581****, 70-78.*

s7 *A. Walcarius and J. Bessiere, Electroanalysis, 1997,* ***9****, 707-713.*